

Acid versus base peptization of mesoporous nanocrystalline TiO₂ films: functional studies in dye sensitized solar cells†

Sarmimala Hore,^{*a} Emilio Palomares,^{bf} Herman Smit,^c Nicolaas J. Bakker,^c Pascal Comte,^d Paul Liska,^d K. Ravindranathan Thampi,^d Jan M. Kroon,^c Andreas Hinsch^{ae} and James R. Durrant^{*b}

Received 5th May 2004, Accepted 29th September 2004

First published as an Advance Article on the web 20th October 2004

DOI: 10.1039/b407963a

We report an analysis of the influence of acid/base conditions employed in the synthesis of TiO₂ nanoparticles upon the performance of dye sensitised photoelectrochemical solar cells fabricated from these particles. The functional properties of the TiO₂ nanoparticles in these devices are investigated by potential step chronoamperometry, transient laser spectroscopy, and photovoltaic device characterisation. We find that base peptization conditions employed in the sol-gel fabrication of the TiO₂ nanoparticles result in a reduction in film electron density under negative applied bias, correlated with slower interfacial recombination losses and a higher device open circuit voltage.

Introduction

The sol-gel chemistry of titania has been the subject of much scientific attention,^{1–5} motivated by the use of nanocrystalline titania for applications ranging from dye sensitized solar cells⁶ to electrochromic windows⁷ and photocatalysis.⁸ The function of the colloidal suspensions of titania, and of nanocrystalline thin films fabricated from such suspensions, have been found to be strongly dependent upon the chemistry employed in nanoparticle synthesis. Such synthetic procedures have been shown to control a wide range of material properties of the resulting films, including particle size and crystallographic phase, film porosity, surface structure, charge and surface area to volume ratio, electron transport properties and optical light scattering.^{9–13} Understanding the origin of the dependence of device function upon synthetic methodologies employed in nanoparticle synthesis is therefore important for device development.

In this paper we focus on one specific aspect of the synthetic methodologies, namely acid/base conditions employed in the peptization of the TiO₂ nanoparticles. Sol-gel preparation of nanocrystalline TiO₂ typically involves the controlled hydrolysis of a Ti(IV) precursor compound such as titanium isopropoxide. The titanium isopropoxide undergoes catalytic hydrolysis or hydrolysis and peptization in the presence of a peptizing agent, which may be either an acid or a base. The peptization step is required in order to de-agglomerate the precipitates formed during hydrolysis; the peptizing agent (0.1 M acid or base) thus ensures the electrostatic stability of the resulting colloidal suspension. The more the pH deviates from the iso-electric point of the nanoparticles (pH of 6.5–7 for TiO₂), the easier the peptization.⁹ Following peptization, the suspension is autoclaved to allow growth of the nanoparticles

to the desired size, often referred to as Ostwald ripening. This autoclaving is dependent both upon the temperature employed and the pH conditions employed in the preceding peptization. Increasing the autoclave temperature has been observed to result in an increase in particle size indicating an increase in dissolution of smaller particles with temperature and corresponding re-precipitation of the dissolved particles on the surface of larger particles while cooling. Crystal growth due to this Ostwald ripening has been reported to be more prominent in basic media compared to acidic conditions.⁹

The electronic properties of nanocrystalline TiO₂ films are dependent upon the extent of protonation of the hydroxylated oxide surface.^{9,14–17} Proton absorption to nanocrystalline metal oxide surfaces are known to shift the positions of the valence band edge maximum and the conduction band edge minimum away from the vacuum level by 59 mV per pH unit of the media in which the film is immersed.¹⁸ Such band energy shifts are known to have a strong influence on the functional properties of nanocrystalline TiO₂ films, including dye binding mode,¹⁹ interfacial electron transfer dynamics²⁰ and photovoltaic device performance.²¹ Studies to date have however largely focused upon the acid/base properties of the electrolyte and sensitizer dye employed and has not focused on the pH conditions employed in the sol-gel synthetic procedures. In this paper we will compare different methodologies based on acid or basic peptization for the synthesis of colloidal nanocrystalline TiO₂ particles and their influence upon the performance of the dye sensitized solar cell (DSSC) devices.

Experimental details

Synthesis of nanocrystalline TiO₂ particles

All nanocrystalline anatase TiO₂ particles studied in this paper were obtained as precipitates from the catalytic hydrolysis of titanium isopropoxide; however, different peptization agents^{9,10,22,23} or catalysts were used as can be seen in Table 1. The steps involved in the synthesis of the colloids can be summarized as follows:

† Electronic supplementary information (ESI) available: XRD data for nanocrystalline TiO₂. See <http://www.rsc.org/suppdata/jm/b4/b407963a/>

*hore@fmf.uni-freiburg.de (Sarmimala Hore)

j.durrant@ic.ac.uk (James R. Durrant)

Table 1 Peptizing agents and autoclave temperature for the TiO₂ colloids

Type of TiO ₂ film	Peptizing reagent	Autoclave temperature/°C
Nanocrystalline TiO ₂ film A	Acetic acid and 0.1 M nitric acid	220
Nanocrystalline TiO ₂ film B	0.1 M nitric acid	230
Nanocrystalline TiO ₂ film C	0.2 M tetramethylammonium hydroxide	180
Nanocrystalline TiO ₂ film D	0.1 M tetramethylammonium hydroxide	230

Nanocrystalline TiO₂ A. 20 ml of titanium isopropoxide were injected into 5.5 g of glacial acetic acid under argon atmosphere and stirred for 10 min. The mixture was then injected into 120 ml of 0.1 M nitric acid under anhydrous atmosphere at room temperature in a conical flask and stirred vigorously. The flask was left uncovered and heated at 80 °C for 8 h. After cooling, the solution was filtered using a 0.45 mm syringe filter, diluted to 5 wt.% TiO₂ by the addition of H₂O and then autoclaved at 220 °C for 12 h. The colloids were re-dispersed with a 60 s cycle burst from a LDU Soniprobe horn as reported before,²⁴ and the resulting solution was concentrated to 12.5% on a rotary evaporator using a membrane vacuum pump at 40 °C. Finally 6.2 wt.% of Carbowax 20 000 was added.

Nanocrystalline TiO₂ B. 125 ml of titanium isopropoxide was injected into 750ml of 0.1M nitric acid, under vigorous stirring. Subsequently the solution was heated to 80 °C for 8 h in order to obtain a complete peptization. To achieve the desired size of the TiO₂, the peptized sol was then subjected to hydrothermal growth in an autoclave for 12 h at 230 °C.^{9,25} Thereafter the particles were washed with ethanol and re-dispersed in the presence of an organic surfactant using a titanium ultrasonic horn. After sonication the resulting solution was concentrated using a rotary evaporator and mixed with Carbowax 20 000 or was transferred into a screen printable paste²⁵ by addition of ethyl cellulose and terpineol.

Nanocrystalline TiO₂ C. As described for the nanocrystalline TiO₂ B, however, the peptizing agent was 0.2 M tetramethylammonium hydroxide and the autoclave temperature was 180 °C.

Nanocrystalline TiO₂ D. As described for the nanocrystalline TiO₂ C using 0.10 M tetramethylammonium hydroxide as the peptizing agent and the autoclave temperature was 230 °C.

Film fabrication and materials characterization

The films were cast on SnO₂ : F conducting glass substrate by using either the doctor blading technique or utilizing screen-printing panels. After deposition, all films were sintered at 450 °C for 30 min such that the organics from the paste were removed. Subsequent to sintering, film thickness was measured with a DEKTAK profilometer, with all film thicknesses being determined to be ~4 μm. The TiO₂ film porosity was measured by the nitrogen adsorption–desorption data and modeled using the Brunauer–Emmett–Teller (BET) equation. TiO₂ nanoparticle size and crystallographic phase were determined by transmission electron micrographs (Zeiss LEO 912 Omega) and X-ray diffraction patterns.

Electrochemistry: potential step chronoamperometry

Chronoamperometry studies of unsensitized films employed a three-electrode photoelectrochemical cell^{26,27} using a platinum foil counter electrode and a Ag/AgCl reference electrode. The electrolyte solution comprised 0.1 M tetrabutylammonium perchlorate, and 0.1 M LiClO₄ in 15 ml anhydrous acetonitrile, prepared with final water content of <20 ppm H₂O determined by a Metrohm 737 Coulometer. The solution was degassed with argon gas prior to and during all optical experiments. The effect of applied bias was reversible in all cases.

The electron densities of the 4 μm unsensitized films of nanocrystalline TiO₂ obtained from different pastes were measured by chronoamperometry an AutoLab PGStat 12 potentiostat as detailed previously.²⁷ The three-electrode cell was left at +200mV vs. Ag/AgCl reference for 10 min to allow equilibrium to be reached. A bias step of –25 mV was applied, the current transient recorded (~50 k samples s⁻¹) and integrated as detailed below. The same procedure was carried out at 100 mV intervals, with the sample held at the new voltage for 5 min prior to each –25 mV step to allow stabilization of the dark current. Electron flow into the film was quantified by integration of the fast charging transient observed following each potential step, yielding a potential dependent film capacitance. Slow charging transients, most probably associated with lithium diffusion–intercalation processes were neglected as discussed previously.²⁷ Integration of these film capacitances allowed calculation of the density of electrons added to the film as function of applied bias.^{26,27}

Transient optical studies of dye sensitized electrodes

Dye sensitization was performed using the ruthenium dye RuL₂(NCS)₂ (chemical name: [bis(2,2'-bipyridyl-4,4'-dicarboxylato)-ruthenium(II) bis-tetrabutylammonium bis-thiocyanate) by soaking the film in a 1 mM solution in 50 : 50 acetonitrile–*tert*-butanol. The dipping time was controlled in order to achieve the desired optical density of 0.3 for all films. Before measurement, all dye sensitized films were rinsed in dry ethanol in order to remove the excess dye which has not been anchored to the film. Finally, the photoelectrode (TiO₂–RuL₂(NCS)₂) was covered with a drop of (1 : 1) polypropylene carbonate and ethylene carbonate to prevent dye oxidation.

Micro-millisecond laser transient absorption studies of the TiO₂–RuL₂(NCS)₂ films were conducted as detailed previously.^{20,28,29} Transient absorption of the dye cation was obtained by optical excitation at 575 nm with pulses from a nitrogen pumped dye laser (<1 ns pulse duration, 0.9 Hz, intensity of about 0.04 mJ cm⁻²). Experiments were conducted

upon photoelectrodes with matched optical densities (0.3) at the excitation wavelength, resulting in ~ 1 absorbed photon per TiO_2 nanoparticle. The resulting photoinduced change in the optical density was monitored with a 100 W tungsten lamp, with 20 nm bandwidth monochromators before and after the sample, a home-built photodiode based detection system and a TDS-220 Tecktronic DSO oscilloscope. For the transient absorption decays presented in this paper, typically about 20–30 laser pulses were averaged for each time scale. No photodegradation of the films was observed after transient absorbance measurements.

Device fabrication and characterization

Dye solar cell devices were fabricated³⁰ as masterplates. Masterplates consist of five individual cells of $5 \times 0.8 \text{ cm}^2$ (SnO_2 : F glass substrate ($8 \Omega \text{ square}^{-1}$)). Since the nanocrystalline TiO_2 film **A** is a water based paste, it was not used to construct the 'masterplate' and was excluded from the I - V characteristic measurement. A screen-print silver paste³¹ was used for the silver strip on each side of each cell to ensure proper current collection within the masterplate. The counter electrode was made by applying a coating of a screen-printable platinum paste and subsequently sintered at $450 \text{ }^\circ\text{C}$ for 30 min. Both electrodes were sealed together with a transparent film of Surllyn 1702 hotmelt foil as the sealing material. The sensitization process was carried out by flushing a 1 mM solution in 50 : 50 acetonitrile-*tert*-butanol of $\text{RuL}_2(\text{NCS})_2$ dye through the masterplate at $40 \text{ }^\circ\text{C}$ for 3 h. The electrolyte (0.6 M tetra butyl ammonium iodide, 0.1 M LiI, 0.1 M I_2 , and 0.5 M 4-*tert*-butyl pyridine in acetonitrile) was filled into the device through the holes on the counter electrode.

Impedance measurements were performed under a bias light illumination of 1000 W m^{-2} from a halogen lamp field. For calibration, a silicon cell was used taking into account the spectral mismatch. Using peltier cooling elements, the cell temperature was kept constant at $25 \text{ }^\circ\text{C}$. The electrical impedance measurements were carried out with the impedance measuring unit (IM 6) from Zahner. Detailed models have been presented earlier³² where electron lifetime in TiO_2 is determined by the minimum frequency of the mid-frequency peak.

Current-voltage measurements were made using a home-built solar simulator under bias light illumination of 1 sun (1000 W m^{-2}) from a halogen lamp field, which was calibrated with a standard silicon cell prior to measurement. Cell temperature was maintained at $25 \text{ }^\circ\text{C}$ throughout the measurement time using peltier cooling apparatus.

Results and discussion

Materials characterization

Material properties of the nanocrystalline TiO_2 films synthesized by the four different synthetic routes are summarized in Table 2, with TEM being shown in Fig. 1. It is apparent that the particle diameters for these four routes differ by almost a factor of four, with a good agreement between the diameters determined from BET and TEM data. XRD data (electronic supplementary information (ESI)†) of the sintered material shows that the TiO_2 particles are all anatase.

The titanium dioxide films reported herein differ from each other in the environment of the hydrothermal synthesis. The effect of pH on the formation of titanium dioxide is similar to that observed for sol-gel derived silica, where base-catalyzed colloids exhibit lower surface areas than those catalyzed with acid.³³ This is consistent with our observation that base peptization is observed to result in larger average particle sizes and lower surface areas, as shown in Table 2. It is furthermore apparent that a higher autoclave temperature results in an increased particle size, as can be seen from comparison of data for nanocrystalline TiO_2 **C** and **D** films **C** and **D**, in agreement with previous reports.⁹

Optical measurements of the saturated (maximal) dye loading achievable for these films provides a complimentary analysis of film surface area, as shown in Fig. 2 and summarized in Table 2. UV-vis steady state optical density measurements of the dye adsorption onto the TiO_2 films shows that nanocrystalline TiO_2 **D** films achieve a lower dye coverage compared with the films sensitized following the acidic synthetic routes, consistent with the lower film surface area determined from the BET analyses and TEM data. It is however furthermore apparent that the acid catalyzed films nanocrystalline TiO_2 **A** and **B** result in similar dye loadings to the base catalyzed nanocrystalline TiO_2 **C**, despite their high surface areas determined from the BET and TEM data, and indicating less favourable dye binding to the acid catalyzed films.

Interfacial electron transfer kinetics

Previous studies have addressed the influence of surface protonation of TiO_2 electrodes upon the interfacial electron transfer.^{20,34,35} Studies have reported^{20,28} that surface proton concentration promotes light induced electron injection from adsorbed sensitizer dyes but at the expense of faster recombination dynamics. It has, for example, previously been shown that for the sensitizer dye $\text{RuL}_2(\text{NCS})_2$, increased protonation of the carboxylic acid groups in the sensitizing solution is correlated with a higher I_{sc} and lower V_{oc} in the

Table 2 Surface area as calculated using BET isotherm obtained from nitrogen absorption and desorption on the TiO_2 films

	BET surface area/ m^2g^{-1}	Porosity(%)	d_{BET}^a /nm	d_{TEM} /nm
Nanocrystalline TiO_2 film A	145	62	11	15
Nanocrystalline TiO_2 film B	93	60	17	15
Nanocrystalline TiO_2 film C	66	45	24	25
Nanocrystalline TiO_2 film D	39	46	40	40

^a Assuming that the particles are spherical, the average diameter is back-calculated from the the BET surface area.

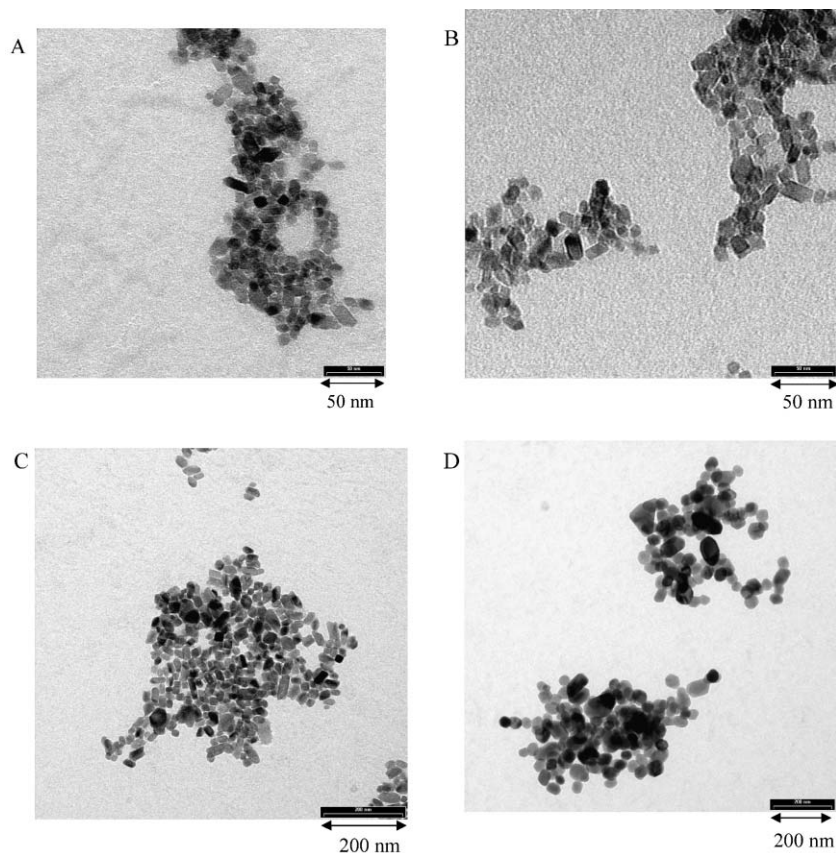


Fig. 1 TEM images of nanocrystalline TiO₂. A, B, C and D are the nanocrystalline TiO₂ A, B, C and D respectively. The average dimensions of nanocrystalline TiO₂ A and B are 15 nm, nanocrystalline TiO₂ C is 25 nm and nanocrystalline TiO₂ D is 40 nm.

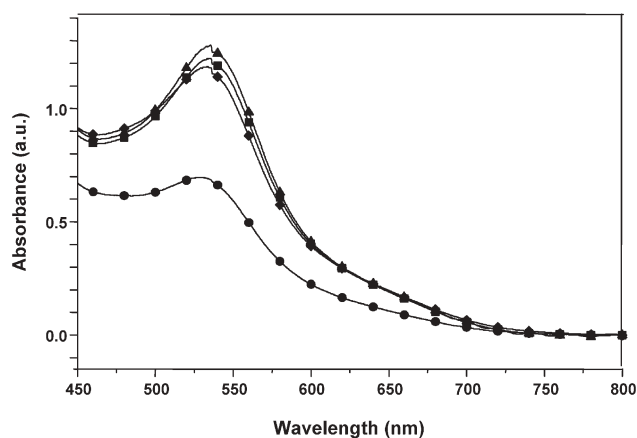


Fig. 2 Absorbance spectra of 4 μm TiO₂ film saturated with the dye Ru(dcbpy)₂-(NCS)₂. (■) Nanocrystalline TiO₂ film A, (▲) nanocrystalline TiO₂ film B, (●) nanocrystalline TiO₂ film C and (◆) nanocrystalline TiO₂ film D as indicated in Table 1.

resulting device.²¹ However, this paper presents for the first time the electron recombination dynamics for different mesoporous TiO₂ films synthesized in different pH environments.

We consider first the interfacial recombination dynamics of dye sensitized TiO₂ films probed by transient absorption

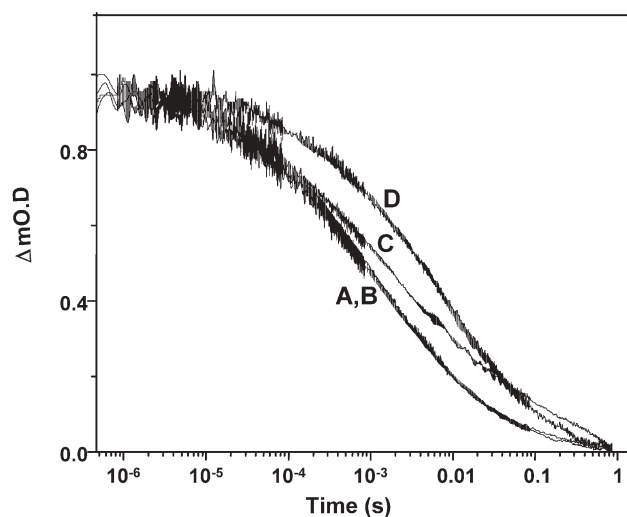


Fig. 3 Transient absorption data monitoring photoinduced absorption of the Ru(dcbpy)₂-(NCS)₂ cation following excitation of the dye adsorbed on mesoporous (A) nanocrystalline TiO₂ film A, (B) nanocrystalline TiO₂ film B, (C) nanocrystalline TiO₂ film C and (D) nanocrystalline TiO₂ film D. The signal decay is assigned to charge recombination of dye cation with electrons in trap/conduction band states of the TiO₂ semiconductor. Optical excitation is at 575 nm and detection registered at 800 nm.

spectroscopy, as illustrated in Fig. 3. Data were collected on films with matched dye loadings, corresponding to OD = 0.3 at 575 nm, the excitation wavelength. It is apparent that the basic synthesis routes result in a significant retardation of the charge recombination kinetics, as summarized by the recombination half times tabulated in Table 3. Similar initial signal magnitudes, and therefore electron injection yields, were observed for all films. We have reported previously that these recombination dynamics are rather insensitive to nanoparticle diameter.²⁷ We therefore assign this retardation of the recombination dynamics to difference in the surface protonation of the films, as we discuss in more detail below.

The influence of applied bias

The recombination dynamics of dye sensitized nanocrystalline TiO₂ films are strongly influenced by the electron occupancy of the conduction band/sub-bandgap trap states of the film, and therefore by the position of the film Fermi level relative to these states.^{20,26,27,36–38} In order to address this behavior, and specifically to address the influence of the acid/base properties of the film upon conduction band/trap state energetic, we conducted electrochemical and transient optical studies of the TiO₂ films under controlled electrical bias in a three electrode photoelectrochemical cell. Electron occupancies n as a function of applied bias were determined by potential step chronoamperometry and correlated with transient absorption measurements of interfacial recombination dynamics. The potential step technique is more detailed in the Experimental section. Electron densities determined by this technique for unsensitized films are shown in Fig. 4.

It is apparent from Fig. 4 that the bias dependence of the electron densities is strongly dependent on the synthetic procedure to obtain the nanocrystalline TiO₂ colloids. Mesoporous TiO₂ films obtained from the colloids synthesized *via* basic catalysis have a reduced dependence of electron density upon applied bias compared with the films obtained from colloids synthesized by acidic hydrolysis. This observation is consistent with our previous studies as a function of acid/base properties of the electrolyte and with our previous studies of the effect of acid/base treatments of preformed nanocrystalline TiO₂ films.^{20,26}

Transient absorption data such as that shown in Fig. 3 were collected as function of applied bias. Fig. 5 shows the bias

Table 3 Comparison of the electron lifetime for the different mesoporous TiO₂ films

Film of TiO ₂	$t_{50\%}/\text{ms}^a$	$t_{50\%}/\text{ms}^b$
Nanocrystalline TiO ₂ film A ^c	1	—
Nanocrystalline TiO ₂ film B	1	3
Nanocrystalline TiO ₂ film C	2	5
Nanocrystalline TiO ₂ film D	5	7

^a $t_{50\%}$ (recombination to the dye cation) are obtained from the transient measurements (Fig. 3) ^b $t_{50\%}$ (recombination to the redox couple in the electrolyte) are the lifetimes derived from electrical impedance spectroscopy measurements carried out under open-circuit condition and under one sun equivalent bias illumination. ^c Impedance are measured only for those devices, which were fabricated from the TiO₂ films cast from screen printable pastes (nanocrystalline TiO₂ B, C and D).

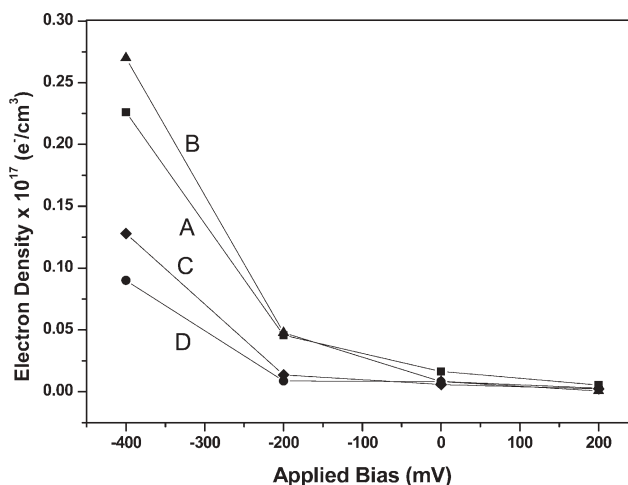


Fig. 4 Electron densities (n) added to the mesoporous TiO₂ (4 μm thickness) films by an applied external bias (Ag/AgCl as reference electrode) in a three-electrode cell with redox inactive electrolyte determined from integration of film capacitances obtained from integration of potential step chronoamperometry data. The letters correspond to the TiO₂ films according to the synthetic routes as reported in Table 1.

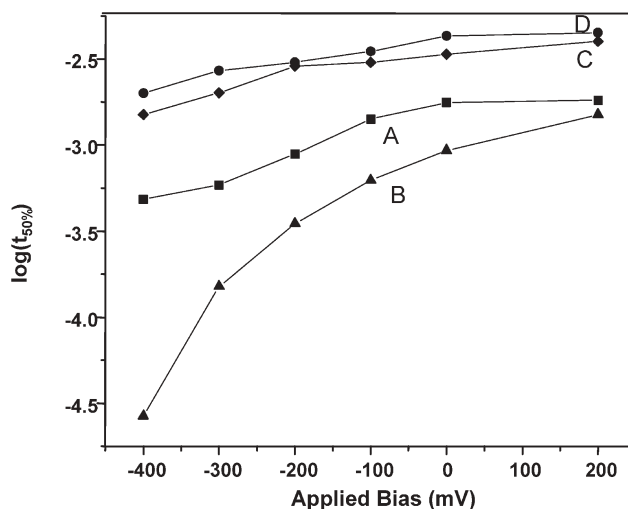


Fig. 5 Dependence of the half time charge recombination $t_{50\%}$ upon applied bias Ag/AgCl electrode reference for Ru(dcbpy)₂–(NCS)₂ dye sensitized TiO₂ films. The $t_{50\%}$ data obtained from transient absorption decays analogously to those shown in Fig. 3 collected as a function of applied bias in a three-electrode photoelectrochemical cell with inactive redox electrolyte.

dependence of the recombination half times ($t_{50\%}$) for the four different film preparations obtained from these data. As can be seen, under negative applied biases, the recombination dynamics exhibit remarkably different dependencies upon applied bias depending on the acid/base peptization conditions employed. At positive biases corresponding to minimal electron density in the TiO₂ films, the acid catalyzed films exhibit a three-fold $t_{50\%}$ consistent with the data taken without external applied bias (Fig. 3 above). Moreover for the acid catalyzed films, the recombination dynamics accelerate more rapidly under negative applied biases, showing a good correlation, as

expected,^{20,39} with the strong dependence of electron density upon applied bias observed for these films in Fig. 4 above. It can be concluded from those experiments that the synthetic routes based on basic peptization are most effective at retarding the interfacial charge recombination, and that this effect is particularly pronounced as the Fermi level is shifted to the negative. This latter observation is of particular importance for device function as such applied potentials correspond to the Fermi levels expected in devices operating load.

Effect of acid/base post-treatment of films

In addition to the potential differences in surface protonation of the films fabricated by the acid and base catalyzed routes, these films differ in average particle size and surface area, with the acid catalyzed films comprising small nanoparticles and higher film surface areas. Our previous studies³⁸ have however shown that neither the film electron densities nor the interfacial recombination dynamics are significantly influenced by nanoparticle size or surface area, suggesting that the effects we observe here originate from the acid/base properties of the films rather than differences in particle size. This issue was further addressed by conducting an acid post-treatment of a base catalyzed film. Before the post-treatment, the film was sintered at 450 °C for 30 min and then dipped into a 1×10^{-5} M acetic acid aqueous solution for 15 min and finally sintered again at 450 °C for 30 min. Chronoamperometric measurements were carried out as above. Fig. 6 shows that the acid post-treatment on the mesoporous TiO₂ films result in an increased dependence of electron density upon applied bias, with this low surface area film exhibiting similar electron densities to those observed for the higher surface area acid catalyzed films.

Device characterisation

The photovoltaic performance of the DSSC was realized by the fabrication of masterplates consisting of five individual

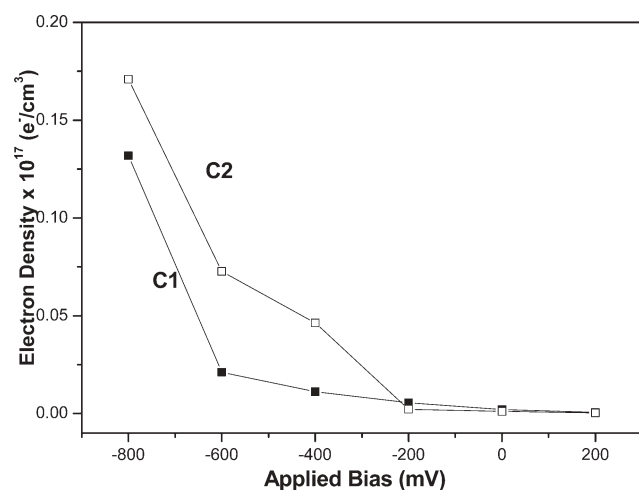


Fig. 6 The figure shows the electron densities added to the nanocrystalline TiO₂ films by an externally applied bias using Ag/AgCl as reference electrode. A nanocrystalline base peptized TiO₂ (curve C1) was treated with 1×10^{-5} M acetic acid solution resulting in electron densities with change in external bias as given by the curve C2.

cells with identical performance employing pastes **B**, **C** and **D**; details of fabrication are detailed above in the experimental section.

Fig. 7 shows the current–voltage characteristics of the DSSC in the dark and under AM 1.5 simulated sunlight, with the performance data being tabulated in Table 4. It is apparent that there is a good correlation between the dark current data and V_{oc} obtained from the data under illumination with recombination data reported above. As expected from the recombination data presented above, the base catalyzed films correspond to a lower dark current and higher V_{oc} . The lower I_{sc} observed for nanocrystalline TiO₂ **D** films are assigned to the lower dye loading for this film. This assignment is supported by transient absorption studies of DSSC with matched dye loadings, which indicated similar injection yields and I_2^- yields for all four films (data not shown).

Conclusions

In this paper we have investigated the effect of acidic vs. basic peptization during the hydrothermal synthesis of nanocrystalline particles of TiO₂ from titanium isopropoxide on the function of dye sensitized nanocrystalline TiO₂ films. We have demonstrated that base sol–gel synthetic routes show retardation of interfacial recombination dynamics. Comparison of Figs. 4 and 5 shows there is a clear correlation between the chronoamperometric and transient absorption data for the

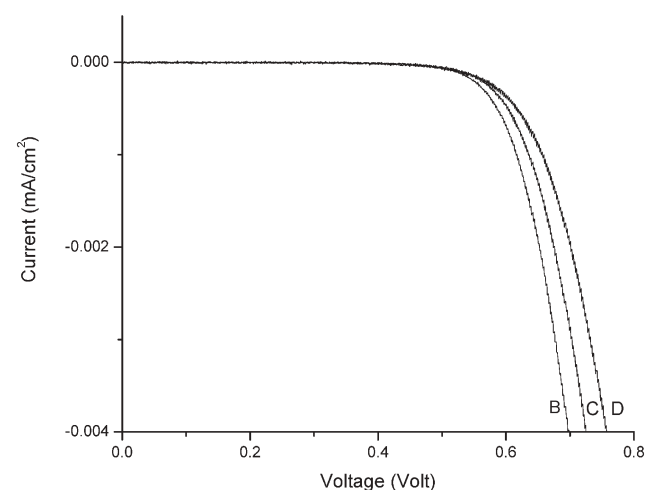


Fig. 7 The dark current data obtained with the masterplates, active area being 4 cm². All measurements were performed on devices constructed as ‘masterplates’ and using screen printable TiO₂ as well as platinum paste. Since the nanocrystalline TiO₂ film **A** is a water based paste, it was not used to construct the ‘masterplate’ and was excluded from the I – V characteristic measurement.

Table 4 I – V data for all dye sensitized nanocrystalline TiO₂ solar cells fabricated on large area (4 cm²) under AM 1.5 simulated sunlight

	$I_{sc}/\text{mA cm}^{-2}$	V_{oc}/mV	$ff^a(\%)$	$\eta(\%)$
Nanocrystalline TiO ₂ film B	10.2	697	61.8	4.5
Nanocrystalline TiO ₂ film C	10.9	718	63.5	4.8
Nanocrystalline TiO ₂ film D	8.13	745	59.1	3.8

^a Fill factor.

different films. The basic films nanocrystalline TiO₂ C and nanocrystalline TiO₂ D exhibit the smallest dependence of both η and $t_{50\%}$ upon bias. The nanocrystalline TiO₂ A and nanocrystalline TiO₂ B films exhibit the strongest dependence of both n and $t_{50\%}$ upon bias.

The difference in device performance for the different films derives from the influence of the acid/basic individual properties of the colloids upon the bias dependence of the film electron density, $n(V)$. This influence can be readily rationalized if we assumed that the acid/base properties of the colloidal solution are retained also in the films. The conduction band energetics of nanocrystalline TiO₂ have been known to exhibit a Nernstian dependence upon electrolyte pH, attributed to protonation/deprotonation of surface oxygen moieties and/or intercalation of protons into the TiO₂ nanoparticles. Following these observations, it might be concluded that optimum device performance will be achieved with mesoporous TiO₂ films derived from basic synthetic routes. However, as a result of the peptization processes, lower film surface area for the basic films results in a lower dye adsorption and therefore lower photocurrent outputs (I_{sc}) on the solar cell devices. It therefore appears possible that the improvement in I_{sc} will be achieved with TiO₂ films post-treatment with acidified titania sources such as TiCl₄ to increase the number of hydroxyl groups onto the TiO₂ surface with minimal effects on the interfacial recombination dynamics.

Acknowledgements

The authors would like to acknowledge Mr A. Green at Imperial College, and Dr S. Baumgärtner at the Freiburg Material Research Center for the synthesis of the colloids. Mr J. Clifford at Imperial College is thanked for laboratory assistance. Dr Ralf Thomann and Dr Martin Ade at Freiburg Material Research Center are gratefully acknowledged for their help with the TEM and the XRD measurements. Prof Michael Grätzel at the Laboratory for Photonics and Interfaces, Swiss Federal Institute of Technology, Lausanne (EPFL) is thanked for helpful discussions. We would also like to thank Dr Gavin Tulloch of Sustainable Technologies International, Australia for useful comments. This work was in part funded by European Union (contract number NNE5-2001-00192 Nanomax).

Sarmimala Hore,^{*a} Emilio Palomares,^{bf} Herman Smit,^c
 Nicolaas J. Bakker,^c Pascal Comte,^d Paul Liska,^d
 K. Ravindranathan Thampi,^d Jan M. Kroon,^e Andreas Hinsch^{ae} and
 James R. Durrant^{*b}

^aFreiburg Materials Research Center, Albert Ludwigs University, Stefan Meier Strasse 21, 79104 Freiburg, Germany.

E-mail: hore@mf.uni-freiburg.de

^bCentre for Electronic Materials and Devices, Department of Chemistry, Imperial College, London SW7 2AY, U.K. E-mail: j.durrant@ic.ac.uk

^cECN Solar Energy, P.O. Box 1, 1755 ZG Petten, The Netherlands

^dLaboratory for Photonics and Interfaces, Swiss Federal Institute of Technology, Lausanne (EPFL), CH 1015, Lausanne, Switzerland

^eFraunhofer Institute for Solar Energy Systems, Heidenhof Straße 2, 79110 Freiburg, Germany

^fInstitut de Ciència Molecular (IcMol). Universitat de València, 46100-Burjassot, Valencia, Spain

References

- B. O'Regan and M. Grätzel, *Nature*, 1999, **353**, 737.
- M. K. Nazeeruddin, A. Kay, I. Rodicio, R. Humphry-Baker, E. Muller, P. Liska, N. Vlachopoulos and M. Grätzel, *J. Am. Chem. Soc.*, 1993, **115**, 6382.
- E. Topoglidis, E. J. C. Collin, E. Palomares and J. R. Durrant, *Chem. Commun.*, 2002, **14**, 1518.
- G. Marci, A. Palmisano, A. Sclafani, A. M. Venezia, R. Campostrini, G. Carturan, C. Martin, V. Rives and S. Solana, *J. Chem. Soc., Faraday Trans.*, 1996, **92**, 819.
- S. Burnside, V. Shklover, C. Barbe, P. Comte, F. Arendse, K. Brooks and M. Grätzel, *Chem. Mater.*, 1998, **10**, 2419.
- A. Hagfeldt and M. Grätzel, *Acc. Chem. Res.*, 2000, **35**, 269.
- A. Hauch, A. Georg, U. Opara Krasovec and B. Orel, *J. Electrochem. Soc.*, 2002, **149**, H159.
- Y. Ohko, T. Tatsuma and A. Fujishima, *J. Phys. Chem. B*, 2001, **105**, 10016.
- C. Barbe, F. Arendse, P. Comte, M. Jirousek, F. Lenzmann, V. Shklover and M. Grätzel, *J. Am. Ceram. Soc.*, 1997, **80**, 3157.
- A. Zaban, S. T. Aruna, S. Tirosh, B. A. Gregg and Y. Mastai, *J. Phys. Chem. B*, 2000, **104**, 4130.
- F. Lenzmann, J. Kreuger, S. Burnside, K. Brooks, M. Grätzel, D. Gal, S. Rühle and D. Cahen, *J. Phys. Chem. B*, 2001, **105**, 6347.
- S. Burnside, J. Moser, K. Brooks and M. Grätzel, *J. Phys. Chem. B*, 1999, **103**, 9328.
- O. Makarova, T. rajh, M. Thurnauer, A. Martin, P. Kemme and D. Crokek, *Environ. Sci. Technol.*, 2000, **34**, 4797.
- H. Gerischer, *Electrochim. Acta*, 1989, **34**, 1005.
- W. D. K. Clark and N. J. Sutin, *J. Am. Chem. Soc.*, 1977, **99**, 4676.
- L. P. Sonntag and M. T. Spitler, *J. Phys. Chem.*, 1985, **89**, 1453.
- A. Zaban, S. Ferrere and B. A. Gregg, *J. Phys. Chem. B*, 1998, **102**, 452.
- A. J. Nozik, *Ann. Rev. Phys. Chem.*, 1978, **29**, 189.
- P. Qu and G. Meyer, *Langmuir*, 2001, **17**, 6720.
- S. A. Haque, Y. Tachibana, R. L. Willis, J. E. Moser, M. Grätzel, D. Klug and J. R. Durrant, *J. Phys. Chem. B*, 2000, **104**, 538.
- M. K. Nazeeruddin, R. Humphry-Baker, P. Liska and M. Grätzel, *J. Phys. Chem. B*, 2003, **107**, 8981.
- I. M. Thomas, *Appl. Opt.*, 1987, **26**, 4688.
- A. Kay and M. Grätzel, *Sol. Energy Mater. Sol. Cells*, 1996, **44**, 99.
- E. Topoglidis, T. Lutz, R. L. Willis, C. J. Barnett, A. E. G. Cass and J. R. Durrant, *Faraday Discuss.*, 2000, **116**, 35.
- M. Späth, P. M. Sommeling, J. A. M. van Roosmalen, H. J. P. Smit, N. P. G. van der Burg, D. R. Mahien, N. J. Bakker and J. M. Kroon, *Prog. Photovoltaics*, 2003, **11**, 207.
- E. Palomares, J. N. Clifford, S. A. Haque, T. Lutz and J. R. Durrant, *J. Am. Chem. Soc.*, 2003, **125**, 475.
- R. Willis, C. Olson, B. O'Regan, T. Lutz, J. Nelson and J. R. Durrant, *J. Phys. Chem. B*, 2002, **106**, 7605.
- S. A. Haque, Y. Tachibana, D. R. Klug and J. R. Durrant, *J. Phys. Chem. B*, 1998, **102**, 1745.
- Y. Tachibana, J. E. Moser, M. Grätzel, D. Klug and J. R. Durrant, *J. Phys. Chem.*, 1996, **100**, 20056.
- A. Hinsch, J. M. Kroon, R. Kern, I. Uhlendorf, J. Holzbock, A. Meyer and J. Ferber, *Prog. Photovoltaics*, 2001, **9**, 425.
- S. Burnside, S. Winkel, K. Brooks, V. Shklover, M. Grätzel, A. Hinsch, R. Kinderman, C. Bradburn, A. Hagfeldt and H. Pettersson, *J. Mater. Sci. Mater.: Electron.*, 2000, **11**, 355.
- R. Kern, R. Sastrawan, J. Ferber, R. Stangl and J. Luther, *Electrochim. Acta*, 2003, **47**, 4213.
- C. Brinker and G. W. Scherer, *Sol-Gel Science*, Academic Press, Boston, 1990.
- J. Martini, J. H. Hodak and G. V. Hartland, *J. Phys. Chem. B*, 1998, **102**, 607.
- H. N. Ghosh, *J. Phys. Chem. B*, 1999, **103**, 10382.
- P. Hoyer and H. Weller, *J. Phys. Chem.*, 1995, **99**, 14096.
- H. L. Wang, J. J. He, G. Boschloo, H. Lindstrom, A. Hagfeldt and S. E. Lindquist, *J. Phys. Chem. B*, 2001, **105**, 2529.
- R. Willis, PhD Thesis, Department of Chemistry, Imperial College, London, 2002.
- J. Nelson, S. A. Haque, D. R. Klug and J. R. Durrant, *Phys. Rev. B: Condens. Matter*, 2001, **63**, 205321.